Research Article
Genetic and Metabolic Diseases

JOURNAL
OF HEPATOLOGY

Microbiota-driven gut vascular barrier disruption is a prerequisite for non-alcoholic steatohepatitis development

Graphical abstract

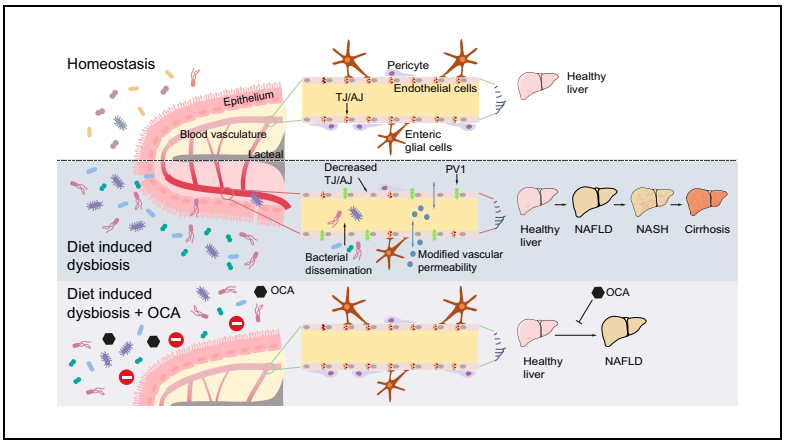

Highlights

- During diet-induced dysbiosis the gut vascular barrier is disrupted.
- Gut vascular barrier disruption is responsible for the translocation of bacteria or bacterial products systemically.
- Inhibiting gut vascular barrier disruption prevents the development of non-alcoholic steatohepatitis.
- Obeticholic acid can control gut vascular barrier disruption both in a preventive and therapeutic way.

Authors

Juliette Mouries, Paola Brescia, Alessandra Silvestri, ..., Luciano Adorini, Giuseppe Penna, Maria Rescigno

Correspondence

maria.rescigno@hunimed.eu
(M. Rescigno)

Lay summary

The incidence of fatty liver disease is reaching epidemic levels in the USA, with more than 30% of adults having NAFLD (non-alcoholic fatty liver disease), which can progress to more severe non-alcoholic steatohepatitis (NASH). Herein, we show that disruption of the intestinal epithelial barrier and gut vascular barrier are early events in the development of NASH. We show that the drug obeticholic acid protects against barrier disruption and thereby prevents the development of NASH, providing further evidence for its use in the prevention or treatment of NASH.

http://dx.doi.org/10.1016/j.jhep.2019.08.005
 J. Hepatol. 2019, 71, 1216–1228

Research Article
Genetic and Metabolic Diseases

JOURNAL OF HEPATOLOGY

Microbiota-driven gut vascular barrier disruption is a prerequisite for non-alcoholic steatohepatitis development

Juliette Mouries[1], Paola Brescia[1], Alessandra Silvestri[1], Ilaria Spadoni[2], Marcel Sorribas[3], Reiner Wiest[3,4], Erika Mileti[5], Marianna Galbiati[6], Pietro Invernizzi[6], Luciano Adorini[7], Giuseppe Penna[1,8], Maria Rescigno[1,2,*]

[1]*Humanitas Clinical and Research Center – IRCCS –, via Manzoni 56, 20089 Rozzano, MI, Italy;* [2]*Humanitas University, Department of Biomedical Sciences, Via Rita Levi Montalcini, 20090 Pieve Emanuele, MI, Italy;* [3]*Maurice Müller Laboratories, Department for Biomedical Research, University of Bern, Bern, Switzerland;* [4]*Department of Visceral Surgery and Medicine, Bern University Hospital, University of Bern, Bern, Switzerland;* [5]*European Institute of Oncology, Department of Experimental Oncology, 20139 Milan, MI, Italy;* [6]*Division of Gastroenterology and Center for Autoimmune Liver Diseases, Department of Medicine and Surgery, University of Milan-Bicocca, Milan, MI, Italy;* [7]*Intercept Pharmaceuticals, New York, NY 10014, USA;* [8]*Postbiotica srl, Via Rita Levi Montalcini, 20090 Pieve Emanuele, MI, Italy*

Background & Aims: Fatty liver disease, including non-alcoholic fatty liver (NAFLD) and steatohepatitis (NASH), has been associated with increased intestinal barrier permeability and translocation of bacteria or bacterial products into the blood circulation. In this study, we aimed to unravel the role of both intestinal barrier integrity and microbiota in NAFLD/NASH development.

Methods: C57BL/6J mice were fed with high-fat diet (HFD) or methionine-choline-deficient diet for 1 week or longer to recapitulate aspects of NASH (steatosis, inflammation, insulin resistance). Genetic and pharmacological strategies were then used to modulate intestinal barrier integrity.

Results: We show that disruption of the intestinal epithelial barrier and gut vascular barrier (GVB) are early events in NASH pathogenesis. Mice fed HFD for only 1 week undergo a diet-induced dysbiosis that drives GVB damage and bacterial translocation into the liver. Fecal microbiota transplantation from HFD-fed mice into specific pathogen-free recipients induces GVB damage and epididymal adipose tissue enlargement. GVB disruption depends on interference with the WNT/β-catenin signaling pathway, as shown by genetic intervention driving β-catenin activation only in endothelial cells, preventing GVB disruption and NASH development. The bile acid analogue and farnesoid X receptor agonist obeticholic acid (OCA) drives β-catenin activation in endothelial cells. Accordingly, pharmacologic intervention with OCA protects against GVB disruption, both as a preventive and therapeutic agent. Importantly, we found upregulation of the GVB leakage marker in the colon of patients with NASH.

Conclusions: We have identified a new player in NASH development, the GVB, whose damage leads to bacteria or bacterial product translocation into the blood circulation. Treatment aimed at restoring β-catenin activation in endothelial cells, such as administration of OCA, protects against GVB damage and NASH development.

Lay summary: The incidence of fatty liver disease is reaching epidemic levels in the USA, with more than 30% of adults having NAFLD (non-alcoholic fatty liver disease), which can progress to more severe non-alcoholic steatohepatitis (NASH). Herein, we show that disruption of the intestinal epithelial barrier and gut vascular barrier are early events in the development of NASH. We show that the drug obeticholic acid protects against barrier disruption and thereby prevents the development of NASH, providing further evidence for its use in the prevention or treatment of NASH.

Introduction

Fatty liver disease is characterized by a series of pathological conditions ranging from hepatic lipid accumulation (steatosis), to hepatocyte degeneration (ballooning), inflammation (steatohepatitis) and, eventually, cirrhosis and hepatocellular carcinoma.[1,2] Fatty liver disease may be the result of long-term excessive ethanol consumption (alcoholic liver disease) or of visceral obesity and metabolic syndrome without ethanol consumption, leading to non-alcoholic fatty liver disease (NAFLD) which can evolve to non-alcoholic steatohepatitis (NASH).[3]

Several factors, likely acting in parallel, contribute to NASH development, including genetic predisposition, epigenetic changes, insulin resistance, abnormal lipid metabolism, oxidative stress, lipotoxicity, mitochondrial dysfunction, endoplasmic reticulum stress, hepatocyte apoptosis, activation of hepatic stellate cells, activation and recruitment of immune cells with production of inflammatory cytokines, altered adipokines, and gut dysbiosis.[4,5]

The important role of the gut microbiota has been clearly established both in preclinical NAFLD/NASH models and in patients with NASH.[6,7] Bacterial overgrowth in the small intestine, as well as qualitative microbiome abnormalities can impair

Keywords: Non-alcoholic fatty liver disease; miRNA; Expression profile; Diagnostic accuracy.
Received 21 December 2018; received in revised form 29 July 2019; accepted 2 August 2019; available online 13 August 2019
* Corresponding author. Address: Humanitas Clinical and Research Center – IRCCS –, via Manzoni 56, 20089 Rozzano, MI, Italy.
E-mail address: maria.rescigno@hunimed.eu (M. Rescigno).

the barrier functions of the intestinal mucosa, leading to enhanced mucosa permeability and subsequent translocation of endotoxin to the bloodstream.[8] Patients with NASH present increased intestinal permeability and small intestinal bacterial overgrowth, which correlate with the severity of steatosis.[9] Similarly, mice deficient in Jam-A, an integral component of tight junctions, which control the paracellular route of solutes and prevent molecules such as lipopolysaccharide (LPS) from crossing the epithelium,[10] are also more susceptible to NASH development.[11] Together, these data suggest that increased gut permeability represents an important mechanism in NASH pathogenesis, leading to the accumulation of endotoxin and bacterial components in the liver, and subsequently to the induction of inflammatory responses, through activation of pattern recognition receptors.

The intestinal epithelial barrier (IEB) is composed of several elements, which are more or less accessible to bacteria and their derivatives. The first line of defense is provided by the mucus layer, thicker in the ileum, cecum and colon where microbes mainly reside.[12] The mucus physically separates the microbiota from the second physical barrier composed of epithelial cells, sealed by tight junctions.[10] We have described that just below the epithelium an additional cellular barrier, the gut vascular barrier (GVB), controls entry into the portal circulation and access to the liver.[13,14] Thus, if a molecule or a microorganism crosses the epithelial barrier, it will remain in the lamina propria, unless the GVB is also impaired. Indeed, for bacteria to reach the systemic circulation the GVB must be disrupted. Enteric pathogens such as *Salmonella typhimurium*, have established strategies to elude the GVB by interfering with the WNT/β-catenin signaling pathway.[14] In addition, the GVB is also disrupted in some pathological conditions such as in celiac disease (in patients with high serum levels of liver aminotransferases),[13] and in patients with ankylosing spondylitis.[15] In the context of NASH, it is unclear if increased intestinal permeability due to disrupted IEB alone is sufficient to induce bacteria and LPS translocation and drive liver damage, or if GVB disruption is also required.

Obeticholic acid (OCA), a derivative of the bile acid chenodeoxycholic acid and a potent agonist of the farnesoid X receptor (FXR)[16] has been shown to play a role in controlling intestinal permeability,[17] gut barrier dysfunction and bacterial translocation.[18] OCA ameliorates disease in patients with type II diabetes mellitus and NAFLD,[19] and in patients with NASH.[20] However, the precise roles of bile acids and FXR in controlling IEB or GVB permeability are still unknown.

Here, we show that patients with NASH display increased intestinal expression of a marker of GVB leakage. This was paralleled by mouse studies showing that one of the earliest events in experimental NASH development is disruption of both the IEB and GVB, which are dependent on dysbiosis induced by HFD. After HFD feeding, the initial event observed at 48 h is IEB disruption followed by GVB damage at 1 week. Both genetic manipulation of the WNT/β-catenin signaling pathway, involved in GVB integrity, and pharmacological treatment with OCA, prevent GVB disruption in mice and protect against NASH development.

Materials and methods

Mice and diets

C57BL/6J mice were purchased from Charles River Laboratories (Calco, Italy). Cdh5(PAC)-CreERT2 mice were used and maintained as previously reported.[13] These mice were crossed to β-catenin$^{lox(ex3)/lox(ex3)}$, containing flox sequences flanking exon 3 of β-catenin (*Ctnnb1*).[49] To induce Cre recombination, mice were fed with tamoxifen-enriched diet (TAM 400) for 2 days and then kept at least 5 days on chow diet (4RF21) to reduce the direct side effects of tamoxifen on the liver. Mice were maintained on chow diet or 10% fat isocaloric (TD.06416) as control diets, 45% lard high-fat diet (HFD, TD.06415), 60% lard HFD (TD.06414), or methionine-choline-deficient diet (MCDD, TD.90262). All diets were purchased from Harlan Laboratories. In some experiments, 30 mg/kg OCA (Intercept Pharmaceuticals, New York) was administered daily via oral gavage or feeding with OCA-supplemented diets.

In all experiments, age- and gender-matched mice were used. All mice were maintained on a 12 h light-dark cycle. Experiments were performed in accordance with the guidelines established in the Principles of Laboratory Animal Care (directive 86/609/EEC) and approved by the Italian Ministry of Health. Mice were not randomized. Investigators were not blinded during experimental mice allocation and outcome assessment.

Analysis of serum parameters

Serum alanine aminotransferase (ALT) activity was measured using a kit (MAK052, Sigma-Aldrich, St. Louis, MO) and LPS was measured by the Limulus Amebocyte Lysate assay (Pierce), both according to the manufacturer's instructions.

Immunofluorescence

Intestinal and liver samples were fixed overnight in paraformaldehyde, L-Lysine pH 7.4 and $NaIO_4$ (PLP buffer). They were then dehydrated in 20% sucrose for at least 4 h and included in OCT compound (Sakura). Alternatively, whole pieces of tissue, were stained directly after fixation in PLP to image whole mount. 10 μm cryosections were rehydrated, blocked with 0.1 M Tris-HCl pH 7.4, 2% FBS, 0.3% Triton X-100 and stained with antibodies recognizing the following proteins: PV1 (clone MECA32, BD Pharmingen, 1:100), ZO-1 (clone ZO1-1A12, Invitrogen, 1:100), CD34 (clone RAM34, eBioscience, 1:50).

Tissues were then incubated with the appropriate fluorophore-conjugated secondary antibody. Before imaging, nuclei were counterstained with 4′,6-diamidin -2-fenilindolo (DAPI). Confocal microscopy was performed on a Leica SP8, using oil immersion objectives with x40 or x63 magnification. Fiji (ImageJ) software package was used for image analysis and fluorescence quantification.

Flow cytometry on intestinal and liver samples

Liver, ileum or cecum samples were flushed and rinsed in cold PBS, then moved to collagenase D (1 mg.ml^{-1}) at 37 °C for 20 min. The reaction was stopped by adding cold EDTA containing FACS buffer (PBS, 10% FBS, 0.1% NaO_3, 5 mM EDTA). Intestinal tissues were crushed and resuspended for FACS staining with the following antibodies: EpCAM, CD31, lyve-1, CD34, ZO-1 for 20 min in the dark. Liver tissues were stained with the following antibodies: CD45, CD3, CD4, CD8, Ly6C, Ly6G, F4/80, CD11b. Cells were acquired on a CANTO II and data were analyzed using FlowJo software.

Fluorescence *in situ* hybridization

For fluorescence *in situ* hybridization (FISH), 6 μm cryosections were rehydrated with 4% PFA and incubated with 10 mg/ml^{-1}

Table 1. Fluorescence *in situ* hybridization probes.

Gene	Fluorochrome	Sequence
Eub338 I	FITC	5′-GCT GCC TCC CGT AGG AGT-3′
Eub338 II	FITC	5′-GCA GCC ACC CGT AGG TGT-3′
Eub338 III	FITC	5′-GCT GCC ACC CGT AGG TGT-3′
non-Eub	Alexa 647	5′-ACT CCT ACG GGA GGC AGC-3′

lysozyme (Sigma) in Tris-HCl 0.1 M (pH 7.4) for 30 min. Slices were then washed and incubated with 5 ng.ml^{-1} of probes (mixed Eub338 and non-Eub in hybridization buffer (0.9 M NaCl, 0.1% SDS) for 90 min at 58 °C in a humid chamber. A mix of probes were used, as shown in Table 1.

Samples were washed with Tris-HCl 0.1 M (pH 7.4) and blocked with Tris-HCl 0.1 M pH 7.4 (2% FBS, 0.3% Triton X) for 30 min at room temperature. Then, they were stained with anti-mouse CD45 (Clone 30-F11) for 1 h, washed and incubated with the appropriate fluorophore-conjugated secondary antibody for 1 h. Before imaging, samples were counterstained with DAPI. For each mouse, 4 to 8 images were taken, and the total number of bacteria was determined. The frequency of bacteria inside or outside CD45^{+} cells was then calculated.

Endothelial leakage analysis from *in vivo* endomicroscopy

Cellvizio® Viewer software (Mauna Kea Technologies) was used to extract the photograms from the endomicroscopy video. Only photograms with vessels in focus and normal blood flow were selected. At least 1 picture per time point was selected and 7 measurements were taken per picture. Measurements were made using Image J as follows: straight lines perpendicular to the vessel were drawn in each vessel within the picture and grey value measured in each pixel along the line. Mean grey value (MGV) of the vessel was calculated and background fluorescence was subtracted. MGV of the immediate extravascular space was calculated in the same way. To avoid bias in our measurements, the same number of pixels were analyzed from the intra and extravascular space in all measurements. We also avoided measuring extravascular spaces where more than 1 vessel could contribute to the fluorescence values. Results are shown as a ratio between mean extravascular fluorescence and mean intravascular fluorescence. When extravasation was too high to distinguish vessels from lamina propria a value of 1 was arbitrarily assigned.

Assessment of bacterial translocation

Intestinal pieces were aseptically collected, content was emptied, and samples were weighted. They were washed for 10 s in sterile PBS, then transferred into sterile PBS with 5% FBS with 0.5 mg/ml^{-1} gentamycin. Intestinal samples were incubated for 30 min in gentamycin at 37 °C, then rinsed in PBS before tissue lysis with 0.5% sodium-deoxycholate. Lysed tissues were plated on Sheep Blood Columbia Agar plates (BD) and incubated for 48 h in aerobic conditions at 37 °C. Colony Forming Units (CFUs) were counted after 24 h incubation, and CFUs per mg of tissue were determined.

Gut microbiota transplantation

Two groups of donor mice (5 per group) were fed Ctrl diet or HFD for 1 week. After 7 days, 1 group was sacrificed, cecal and colon content was harvested, pooled and gavaged into recipient mice (5 per group). The next days, feces were harvested from the second donor groups and gavaged into recipient mice (0.05 mg/mouse), for 2 consecutive days. One week after the first gavage, the intestines from recipient mice were harvested in PLP.

Human specimens

Endoscopic specimens were collected from the colons of 9 patients with NASH (Table 2) and 5 healthy controls. Patients were categorized as having NASH by evaluating the presence of steatosis, lobular inflammation, and hepatocellular ballooning on liver biopsies. These analyses were scored according to the Pathology Committee of the NASH Clinical Research Network.[50]

All tissues were obtained from patients, after signing an informed consent, and handled anonymously. Comitato Etico ASST Monza approved the study protocol.

Immunohistochemistry and tissue staining

PV1 immunohistochemistry was performed on 4 mm formalin-fixed paraffin embedded human intestinal tissue sections. Following deparaffinization and re-hydration steps, the antigen is retrieved with 1 mM EDTA (pH 8) at 95 °C for 50 min and endogenous peroxidases were quenched with 3% H_2O_2.

Slides were blocked (TBS 1x, BSA 2%, serum 2%, Tween20 0.02%) for 20 minutes at room temperature. Polyclonal antibody against human PV1 protein (Sigma-Aldrich, 1:200) was used for staining colon biopsies. Secondary anti-rabbit horseradish peroxidase antibody (DAKO, K4003) was used and signal was detected using 3,3′diaminobenzidine.

Sirius red (Sigma) was performed on 4 mm formalin-fixed paraffin embedded mouse liver tissue sections according to manufacturer protocol. Oil Red O (ORO) (Sigma) was performed on PLP buffer fixed OCT embedded frozen liver sections according to manufacturer's protocol.

Bright field images were acquired with virtual slide microscope VS120 (Olympus) using dry objective with x20

Table 2. Demographic characteristics patients with NASH.

Patient	Sex	Age	Steatosis	Lobular inflammation	Hepatocellular ballooning	Total NAS score
1	M	50	1	1	0	2
2	M	62	3	1	1	5
3	M	77	n.d.	n.d.	n.d.	n.d.
4	M	72	3	2	1	6
5	F	62	1	2	0	3
6	M	70	1	2	0	3
7	F	75	n.d.	n.d.	n.d.	n.d.
8	M	52	2	1	0	3
9	M	35	3	1	0	4

NAS, NAFLD activity score; NASH, non-alcoholic steatohepatitis; n.d., not determined.

magnification. BIOP VSI reader on Fiji (ImageJ) software was used for image analysis.

Statistical analysis

From 3 to 5 mice per group were included in all experiments to ensure statistical significance, as the model is reproducible, and the mouse population is homogenous.

Statistical significance was determined with an unpaired 2-tailed *t* test, 1-way or 2-way ANOVA test, as indicated in the figure legend. Error bars indicate SEM on all graphs. Prism 5.0 (Graphpad, La Jolla, CA) was used for all statistical analyses. AUC (Area Under the Curve) calculation was also determined using Prism software.

Results

Intestinal epithelial and vascular barrier disruption are early events in high-fat dietary regimen

HFD is a dietary regimen rich in animal saturated fat (45% lard), known to induce a metabolic disorder leading to insulin

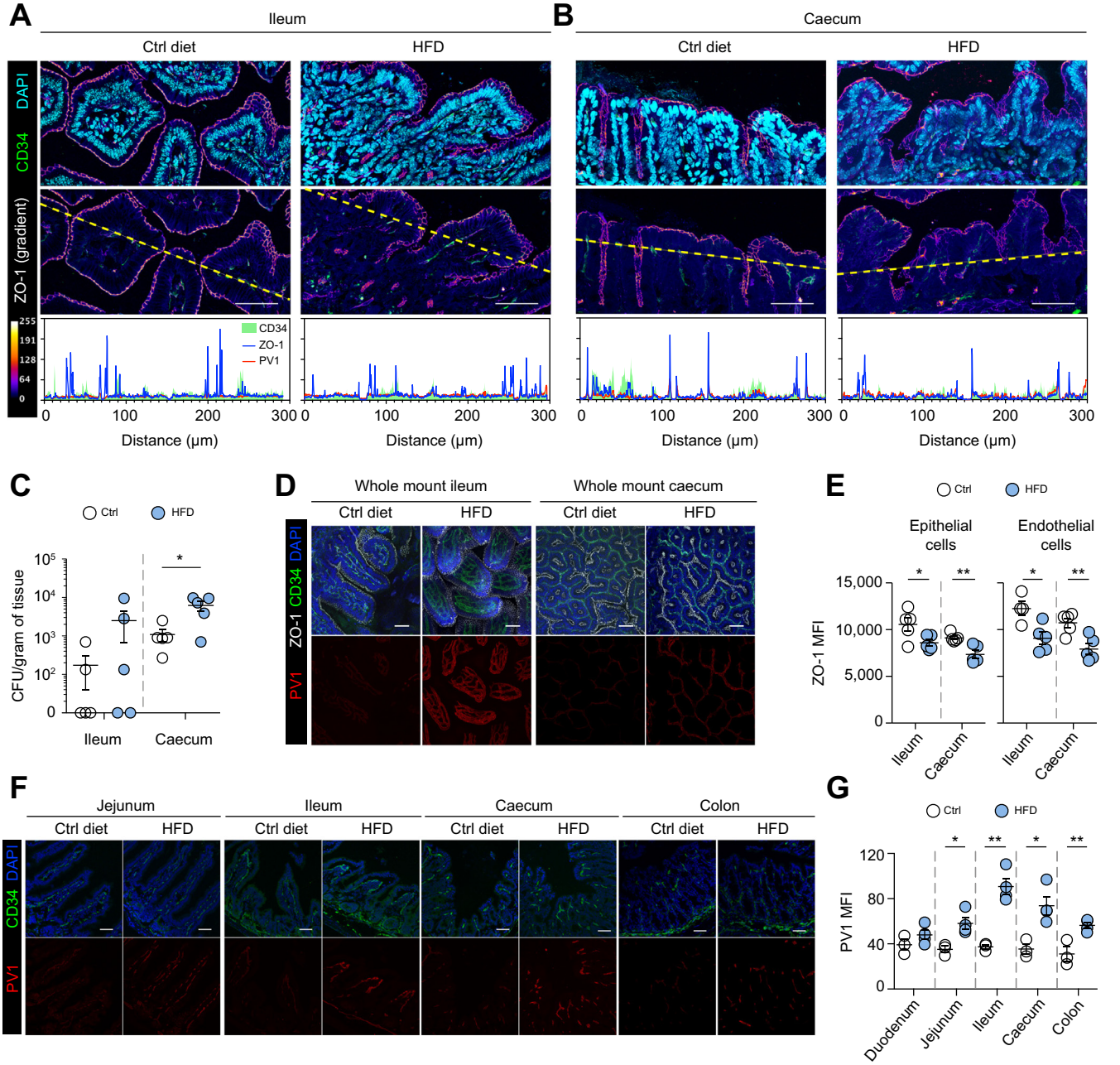

Fig. 1. One week of HFD feeding is sufficient to induce leakage of the gut vascular barrier. (A–C) Mice were fed with control (Ctrl) diet or HFD for 48 h before their intestines were harvested. (A) Ileum and (B) cecum sections were stained for CD34 (green), PV1 (red), ZO-1 (gradient), and DAPI (cyan) expression. First row shows the merged images. Second row is only showing CD34 and ZO-1 with a gradient (as indicated in the legend), and a dotted line indicating where fluorescent intensity was measured. Scale bar indicates 50 μm. Third row displays the intensity profiles of each marker. CFUs in ileum and cecum were determined, as indicated in C, as described in Materials and methods. (D–G) Intestine from mice fed for 1 week was imaged as (D) whole mount or (F) sections. (E) Cell suspension from cecum and ileum was also analyzed by FACS for ZO-1 expression. (G) Quantification of PV1 was performed on $CD34^+$ area. Scale bar indicates 50 μm. $^*p$ <0.05; $^{**}p$ <0.005; unpaired 2-tailed *t* test. CFUs, colony-forming units; HFD, high-fat diet; MFI, mean fluorescence intensity.

resistance, type II diabetes and NASH in C57BL/6 mice.[21] We first assessed whether HFD, compared to an isocaloric diet regimen where calories are provided primarily by starch, could alter the IEB and GVB. As a sign of epithelial damage, we analyzed the expression of tight junction protein ZO-1 and bacterial translocation in the ileum and cecum lamina propria of HFD versus control diet-fed C57BL/6 male mice at an early time point after feeding (48 h). As shown in Fig. 1A–C, at 48 h we detected reduced expression of the tight junction protein ZO-1 on epithelial cells (Fig. 1A,B). The mean fluorescence intensity of intestinal epithelial cell-associated ZO-1 (blue line) was much lower in the HFD than in control fed mice (Fig. 1A,B, profile plots, last row). This correlated with increased bacterial translocation to the ileum and cecum lamina propria (Fig. 1C). A reliable marker

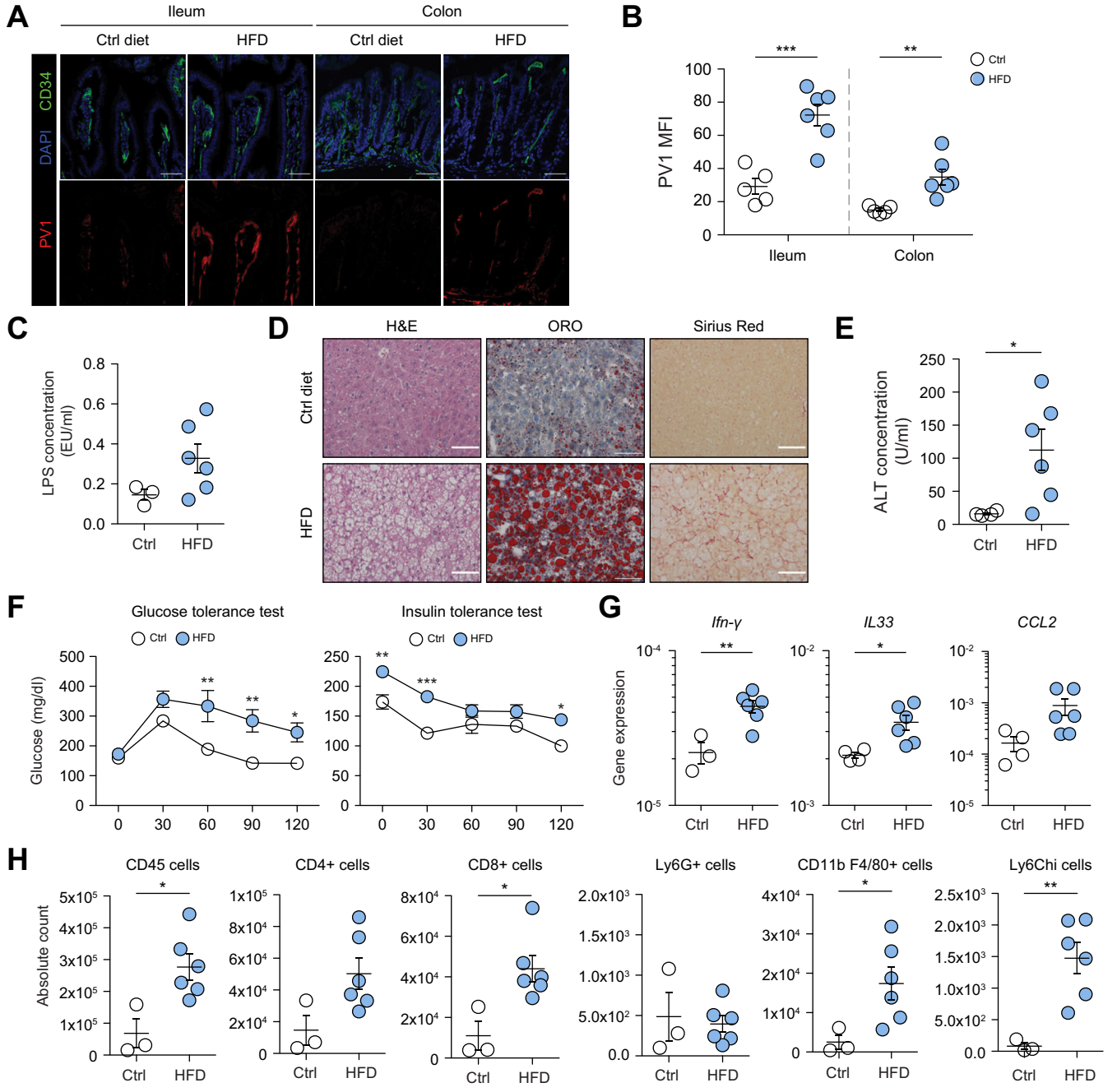

Fig. 2. Long-term HFD feeding induces GVB disruption and liver inflammation and steatosis. (A–H) Mice were fed with control (Ctrl) diet or HFD for 24 weeks before their intestines and livers were harvested. (A) Ileum and colon sections were stained for CD34 (green), PV1 (red) and DAPI (blue) expression, scale bar indicates 50 μm. (B) Quantification of PV1 MFI was performed on $CD34^+$ area. (C) LPS levels were measured in the serum of Ctrl or HFD-fed mice. (D) Liver sections were analyzed by H&E, ORO or Sirius Red staining, as indicated. Scale bar indicates 100 μm. (E) ALT serum concentration in Ctrl or HFD-fed mice. (F) Glucose tolerance test and insulin tolerance test were performed after 6 h of fasting and intraperitoneal injection of glucose (2 g/kg mouse) and insulin (0.2 IU/kg mouse) respectively. (G) Analysis of gene expression (normalized to PPIA gene) by qPCR in the liver of Ctrl or HFD-fed mice. (H) FACS staining of immune cells in the liver of Ctrl or HFD-fed mice represented as absolute numbers. $^*p$ <0.05; $^{**}p$ <0.005; $^{***}p$ <0.0005; unpaired 2-tailed *t* test or 2-way ANOVA in panel F. ALT, alanine aminotransferase; GVB, gut-vascular barrier; HFD, high-fat diet; LPS, lipopolysaccharide; MFI, mean fluorescence intensity; ORO, Oil Red O.

of GVB disruption is the accessibility of plasmalemma vesicle-associated protein 1 (PV1), an integral membrane protein associated to the diaphragms of endothelial fenestrae, by the antibody MECA-32.[13,14] We found that at 48 h there was no increased exposure of PV1 in any of the conditions tested (Fig. 1A,B, red line, profile plots, last row). However, at 1 week after initiation of HFD, ZO-1 was downregulated in both epithelial (EpCAM$^+$) and CD34$^+$ blood endothelial cells, as assessed by confocal (Fig. 1D) and FACS (Fig. 1E) analysis in the cecum and ileum. Also, in the colon we observed a reduction of ZO-1 expression in both endothelial and epithelial cells, although not reaching a statistically significant difference compared to control mice (data not shown). The expression of other tight junction proteins such as Occludin, Claudin-3 and Claudin-5 was not altered by HFD feeding (Fig. S1). At the same time, PV1 was significantly upregulated in the ileum and cecum of HFD-fed mice (Fig. 1F,G). A similar scenario was observed in the jejunum and colon (Fig. 1F,G).

These results suggest a sequential series of events following HFD treatment: first the disruption of the IEB which allows translocation of bacteria, or their molecular determinants, from the lumen and subsequent impairment of the GVB. We thus analyzed whether a high oral load of pathogen-associated molecular patterns may mimic the observed effect. Injection of LPS via oral gavage to mice induced a dramatic reduction of ZO-1 expression at 24 h, indicating IEB damage; at 48 h LPS induced a subsequent increase of PV1 expression in the endothelium, which was dose-dependent, indicating GVB disruption when the endothelium is exposed to high concentrations of LPS (Fig. S2).

We then analyzed whether at later times during HFD feeding, when insulin resistance is established, the GVB is

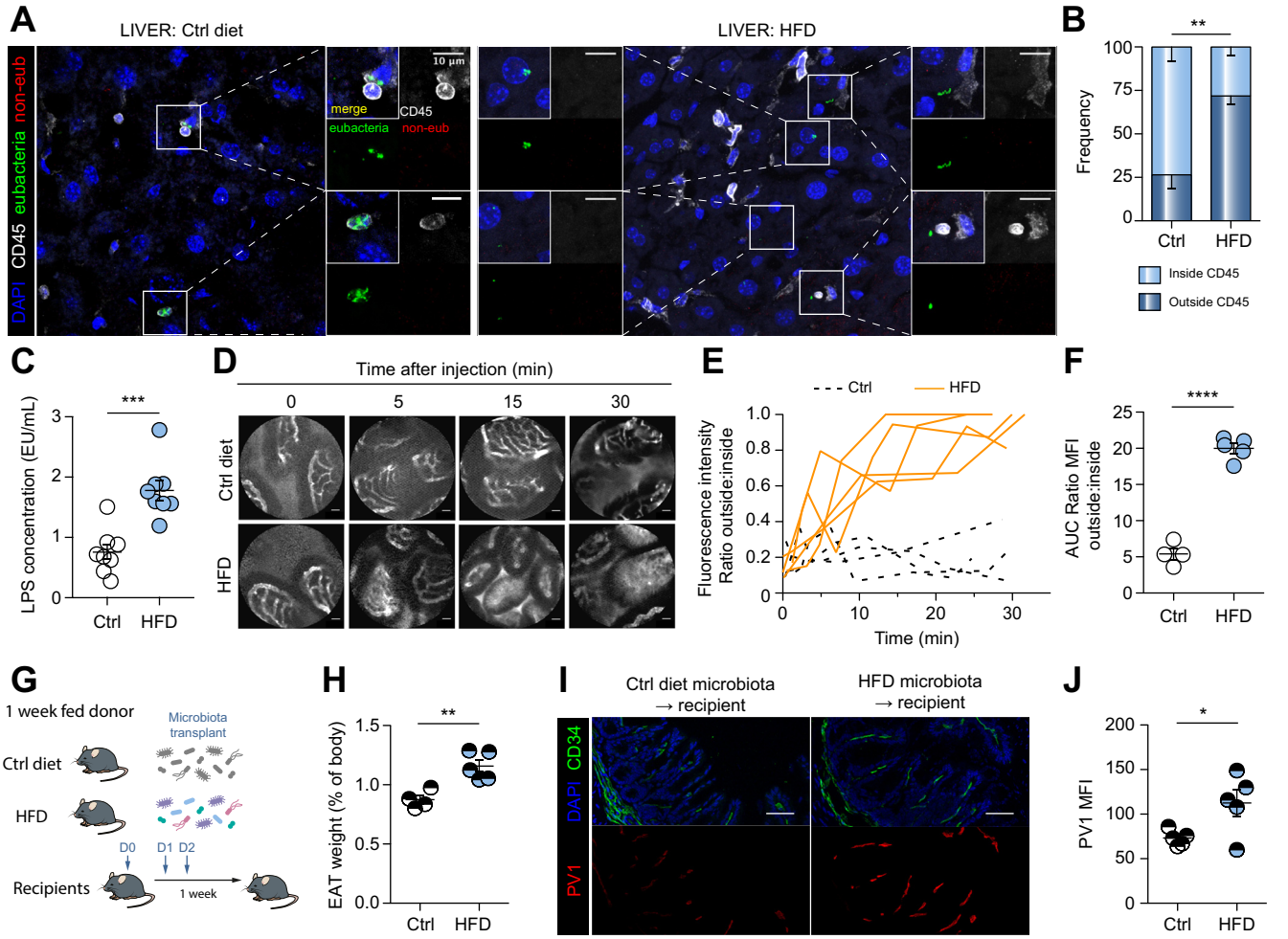

Fig. 3. GVB leakage allows the passage of large molecules and bacteria. (A–F) Mice were fed with control (Ctrl) diet or HFD for 1 week, and (A) liver sections were submitted to eubacteria (green) and non-eub (red) FISH, before CD45 (white) and DAPI (blue) staining. Side images show merged and individual staining of enlarged areas demarcated by squares in the main picture, scale bar indicates 10 µm. (B) Bacteria were enumerated for each mouse, and percentage of bacteria inside or outside CD45$^+$ cells was determined. (C) LPS levels were measured in the serum of 1-week HFD-fed mice. (D–F) One-week-fed mice were injected i.v. with 500 kDa FITC-dextran and imaged by intravital probe-based confocal microscopy. Representative photograms from the endomicroscopy video at indicated time points are shown in C, scale bar indicates 20 µm. Quantification of the fluorescence was measured as described in materials and methods. (E) The fluorescence ratio was plotted over time and (F) the AUC was calculated for each individual mouse. Fecal microbiota transplant of 1-week-fed donors was performed according to the schema in G and as described in materials and methods. Recipients were analyzed 1 week later. (H) Organ and body weight were determined and EAT weight (% of body) was calculated. (I) Cecum was stained for PV1 (red), CD34 (green) and DAPI (blue), scale bar indicates 50 µm. Quantification of PV1 was performed on CD34$^+$ area (j). *p <0.05; **p <0.005; ***p <0.0005; ****p <0.0001 unpaired 2-tailed t test. AUC, area under the curve; EAT, epididymal adipose tissue; FISH, fluorescence *in situ* hybridization; GVB, gut vascular barrier; HFD, high-fat diet; LPS, lipopolysaccharide; MFI, mean fluorescence intensity.

compromised, and whether this correlates with an increased inflammatory response within the liver. To this aim, mice were fed a diet containing 60% fat (60% HFD) which, unlike 45% HFD, induced an inflammatory response in our animal facility. We found that also in mice fed 60% HFD for 24 weeks the GVB was disrupted, as assessed by PV-1 staining both in the ileum and colon (Fig. 2A,B). This correlated with an increase of LPS translocation in the bloodstream (Fig. 2C). The induction of NASH was confirmed by the presence of lipid accumulation in the liver (Oil Red O staining, Fig. 2D), fibrosis (Sirius red staining for collagen fibers, Fig. 2D) and increased serum aminotransferases (ALT, Fig. 2E). The mice also displayed insulin resistance, as assessed by an altered response to glucose and insulin tolerance tests (Fig. 2F). Clear signs of inflammation in the liver were observed, with an increase of inflammatory cytokines and chemokines (*Ifn-γ*, *Il33* and *Ccl2*) (Fig. 2G) and of immune cells (CD45+ cells), in particular CD4+ and CD8+ T cells, monocytes and macrophages (Fig. 2H).

These results indicate that, early after HFD feeding, IEB disruption leads to bacterial translocation, which is followed by GVB disruption. GVB disruption is maintained throughout the development of NASH and inflammation-driven insulin resistance and obesity.

Increased vascular permeability allows bacterial translocation to the liver

Having observed bacteria translocation across the epithelium, we hypothesized that if the GVB was effectively disrupted, as shown by increased PV1 expression, we should also detect bacteria in the liver. To detect the presence and the location

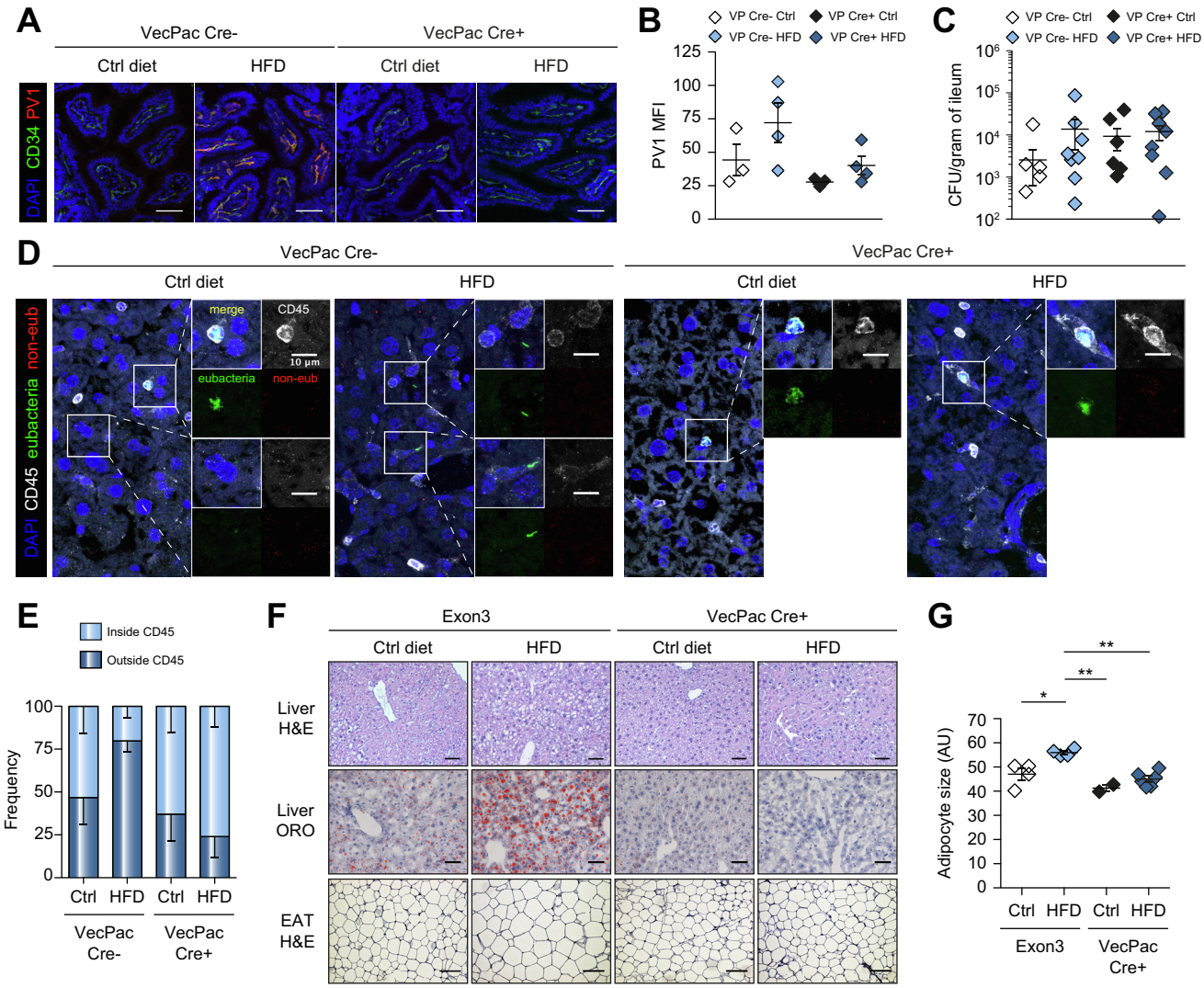

Fig. 4. Endothelium-specific gain-of-function mice are resistant to steatosis induction. (A–E) β-catenin gain-of-function mice were fed for 2 days with tamoxifen to induce recombination, before being fed with either Ctrl diet or HFD for 1 week or (F,G) 18 weeks. (A,B) Ileum sections were analyzed for the expression of PV1, scale bar indicates 50 µm; and (C) CFUs were determined. (D,E) Liver sections were submitted to eubacteria (green) and non-eub (red) FISH hybridization before CD45 (white) and DAPI (blue) staining. Side images show merged and individual staining of enlarged areas demarcated by squares in the main picture, scale bar indicates 10 µm. Bacteria were enumerated for each mouse, and (E) the percentage of bacteria inside or outside CD45$^+$ cells was determined. (F) After 18 weeks of feeding, EAT and liver sections were analyzed by H&E or ORO staining, as indicated. First row, liver hematoxylin and eosin staining, scale bar indicates 100 µm; second row, liver ORO staining, scale bar indicates 50 µm; third row EAT hematoxylin and eosin staining, scale bar indicates 50 µm. Adipocyte diameter was measured and displayed in G. $^*p$ <0.05; $^{**}p$ <0.005; Bonferroni 1-way ANOVA. CFUs, colony-forming units; EAT, epididymal adipose tissue; FISH, fluorescence *in situ* hybridization; HFD, high-fat diet; LPS, lipopolysaccharide; MFI, mean fluorescence intensity; ORO, Oil Red O.

of bacteria, we performed FISH analysis with probes to detect eubacteria 16S rRNA region and immunostaining for CD45 to detect immune cells. We found that livers of control diet-fed mice were harboring few bacteria, which were mostly within CD45$^+$ immune cells, although it is unclear if these were resident liver bacteria or were shuttled from elsewhere (Fig. 3A, B). By contrast, in the livers of HFD-fed mice, bacteria were found in the parenchyma, outside immune cells (Fig. 3A,B), suggesting their free migration to the liver. In agreement with the increased bacterial translocation, LPS levels in the serum of mice fed with HFD were consistently higher than in mice fed with control diet (Fig. 3C).

To functionally assess whether the GVB was effectively disrupted, we carried out fluorescent endomicroscopy using the Cellvizio® technology.[22] Mice were fed with HFD or control diet for 1 week before a high molecular weight FITC-dextran fluorescent probe (500 kDa), resembling the size of a bacterium, was administered intravenously. The capacity of the dye to extravasate into the lamina propria of the ileum was evaluated by fluorescent intravital endomicroscopy. Using this approach, we address only GVB permeability, as the dye would migrate from the blood lumen into the lamina propria. Confirming that increased permeability leads to bacterial translocation (Fig. 3A,B), we found that in HFD-fed mice, but not control diet-fed mice, the intestinal blood vessels had become permeable to the dye (Fig. 3D–F). Interestingly, despite increased weight and adipose tissue size, the observed GVB and IEB disruptions preceded any sign of liver steatosis, adipocyte enlargement, or pancreatic damage, as shown by ORO staining or histology (Fig. S3).

Similar results were obtained following 6 weeks of HFD feeding in female C57BL/6 mice, which display delayed disease development and a broader window of pre-diabetic state[23] (Fig. S4A). Also in this case, mice increased their body mass and visceral adipose tissue (Fig. S4B) and, in the absence of liver steatosis or insulin resistance (Fig. S4C,D), they displayed increased PV1 and reduced ZO-1 expression on intestinal blood endothelial cells (Fig. S4E). Taken together, the increased endothelial permeability and bacterial translocation during HFD indicate that GVB disruption is an early event in NASH development, preceding liver steatosis.

A dysbiotic microbiota can affect GVB integrity

It is known that HFD induces a change in microbiota composition in mice.[24] Thus, having observed that IEB and GVB disruption are early events prompted by HFD, we assessed if the diet-induced microbiota changes were responsible for GVB disruption, by carrying out fecal microbiota transplantation (FMT). The possible involvement of the microbiota in controlling the GVB is suggested by our observation that adult germ-free mice show increased expression of PV1 compared to SPF mice (data not shown). However, microbiota reconstitution of germ-free mice does not lead to PV1 normalization, suggesting an impairment in GVB which cannot be corrected by the microbiota, at least in adult mice (data not shown). Furthermore, GF mice are resistant to HFD-induced NASH, confirming our hypothesis that bacterial translocation across the intestine is responsible for NASH development.[25] For these reasons we performed FMT in SPF mice. Donor mice were fed HFD or control diet, and after 1 week, their microbiota from the feces and

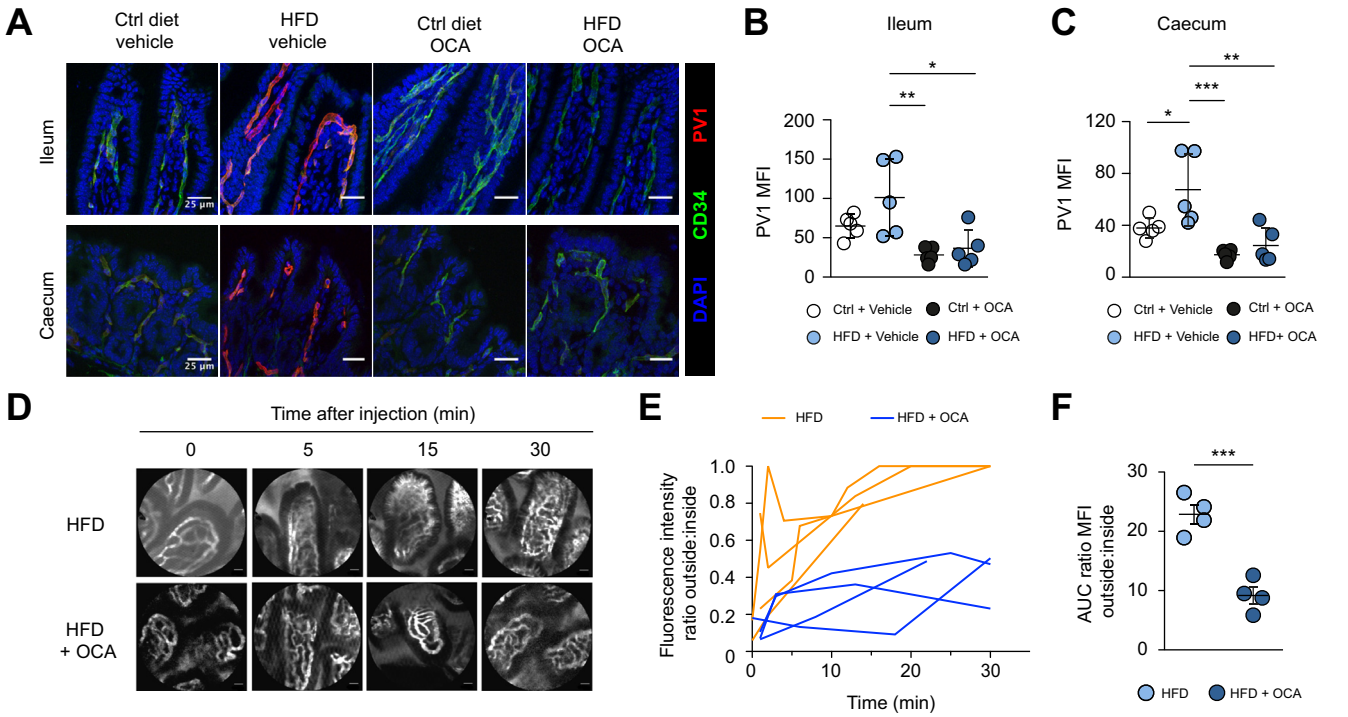

Fig. 5. FXR activation controls GVB tightness. (A–F) Mice were fed with Ctrl diet or HFD supplemented or not with OCA for 1 week. (A–C) Ileum and cecum sections were analyzed for PV1 expression, scale bar indicates 25 μm. (D–F) Alternatively, mice were i.v. injected with 500 kDa FITC-dextran and imaged by intravital probe-based confocal microscopy. Representative photograms from the endomicroscopy video at indicated time points are shown in D, scale bar indicates 20 μm. (E) The outside/inside fluorescence ratio was plotted over time and (F) the AUC was calculated for each individual mouse. *p <0.05; **p <0.005; ***p <0.0005; Bonferroni 1-way ANOVA (B,C). ***p <0.0005; unpaired 2-tailed t test (F). AUC, area under the curve; GVB, gut vascular barrier; HFD, high-fat diet; LPS, lipopolysaccharide; MFI, mean fluorescence intensity; OCA, obeticholic acid.

associated mucus (see Methods) were collected and transferred into recipient mice (Fig. 3G). Recipient mice were maintained on a standard chow diet, and a week later analyzed for weight gain and sacrificed to collect their organs. As shown in Fig. 3H, mice receiving FMT from HFD-fed mice displayed increased epididymal adipose tissue (EAT) even if they were fed a standard diet, compared to recipients receiving FMT from mice under control diet. In addition, the GVB of mice treated with FMT from HFD-fed mice displayed increased PV1 expression (Fig. 3I,J). Together, these results indicate that HFD modifies the microbiota, inducing dysbiosis that affects the GVB and correlates with increased intestinal blood vessel permeability.

GVB disruption is a prerequisite for NASH induction

Having observed a disruption of the GVB during HFD, we assessed its role in NASH induction. We have previously shown that interference with the WNT/β-catenin signaling pathway in endothelial cells is a mechanism adopted by *Salmonella typhimurium* to induce GVB disruption.[13] We thus forced β-catenin activation in mice only in endothelial cells, using VE-cadherin Cre (*Cdh5*(PAC)-creERT2) mice crossed to β-cat$^{lox(ex3)/lox(ex3)}$, which contain 2 flox sequences flanking exon 3 of the β-catenin gene. Upon tamoxifen administration, in Cre^{+} mice, exon 3 of β-catenin is deleted, leading to a non-degradable form of β-catenin and a gain-of-function (GOF) phenotype.[13] When β-catenin is constitutively activated, the GVB cannot be disrupted.[13] We used, as controls, either exon3 floxed mice (β-cat$^{lox(ex3)/lox(ex3)}$), or Cre- littermate mice, born from the same mothers (sharing the same microbiota), with similar results. Cre^{+} and Cre^{-} mice were fed control diet or HFD for 1 week, as above, and PV1 accessibility was assessed. As shown in Fig. 4A,B, HFD was not capable of inducing PV1 upregulation in β-catenin GOF mice. As expected, as the GOF is only occurring in endothelial cells, leaving epithelial cells unaffected, bacteria could still translocate into the ileum and cecum after HFD (Fig. 4C and data not shown).

We next analyzed bacterial translocation to the liver, and found that Cre^{+} β-catenin GOF mice, when fed HFD, resembled

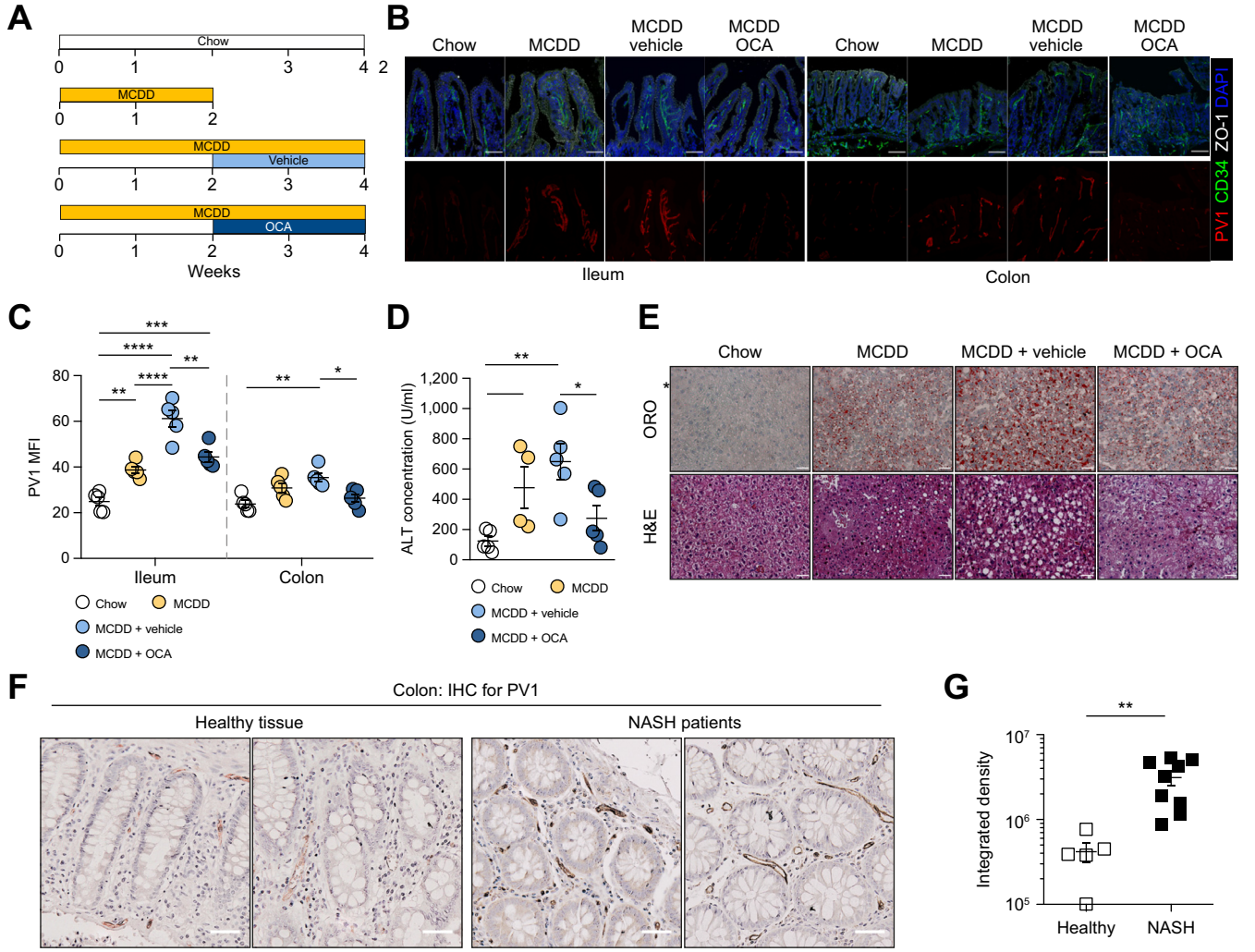

Fig. 6. Obeticholic acid treatment ameliorates the GVB and liver damage in MCDD model. (A) Mice were fed with chow diet or MCDD for 2 weeks before OCA or its vehicle was administered. (B) Ileum and colon sections were stained for CD34 (green), PV1 (red), ZO-1 (white), and DAPI (blue) expression, scale bar indicates 50 μm. (C) Quantification of PV1 MFI was performed on CD34^{+} area. (D) Measurement of ALT concentration in the serum of mice fed with chow or MCDD and treated or not with OCA. (E) Liver sections were analyzed by H&E or ORO staining, as indicated. Scale bar indicates 100 μm. (F) Healthy tissue or colon from patients with NASH were stained for PV1, scale bar indicates 50 μm. (G) PV1 staining was quantified for both groups. $^{*}p$ <0.05; $^{**}p$ <0.005; $^{***}p$ <0.0005; $^{****}p$ <0.0001; unpaired 2-tailed *t* test or 1-way ANOVA in panel C. ALT, alanine aminotransferase; GVB, gut vascular barrier; MCDD, methionine-choline-deficient diet; MFI, mean fluorescence intensity; NASH, non-alcoholic steatohepatitis; OCA, obeticholic acid; ORO, Oil Red O.

control diet-fed mice (Fig. 4D,E). In HFD-fed Cre$^-$ mice, we could find free bacteria, not internalized by CD45$^+$ immune cells, whereas most of the bacteria detected in the Cre$^+$ mice were within immune cells. This suggests that, in the presence of an intact GVB, translocation of free bacteria into the liver is impeded. When mice were fed HFD for a longer period, to induce liver steatosis, we observed that Cre$^+$ GOF mice displayed no adipocyte enlargement (Fig. 4F,G) and were completely protected from NAFLD, as shown by histology and the lack of lipid accumulation in the liver (Fig. 4F). In Cre$^+$ GOF mice we also observed an improvement in blood glucose levels induced by HFD (Fig. S5A).

Interestingly, HFD feeding for 10 days led to leukocyte recruitment, including CD8$^+$ T cells and inflammatory monocytes, in the adipose tissue of Cre$^-$ but not Cre$^+$ GOF mice (Fig. S5B,C). Together, these results indicate that impairment of IEB alone is not sufficient to induce NASH and that GVB disruption is also required.

The FXR agonist obeticholic acid as a pharmacologic treatment to protect GVB integrity

As mentioned above, OCA has been shown to ameliorate NASH in animal models[26] and in patients.[19,20] OCA also protects against inflammation-induced epithelial permeability via FXR-dependent mechanisms[17,18] and reduces bacterial translocation to mesenteric lymph nodes in cholestatic[18] and in cirrhotic rats.[27] We thus evaluated whether OCA could affect HFD-induced intestinal permeability by targeting the GVB. We fed mice with HFD or control diet and orally administered OCA (30 mg/kg for 1 week). Interestingly, we observed that OCA inhibits the upregulation of PV1 (Fig. 5A–C) and increases ZO-1 expression (Fig. S6), suggesting a greater GVB tightness. We then asked if controlling PV1 expression leads to GVB protection. Mice were fed with HFD or control diet for 1 week, with or without OCA, and then administered intravenously with the high molecular weight (500 kDa) fluorescent probe FITC-dextran. We found that OCA administration reduced extravasation of the dye, suggesting that OCA functionally protects the GVB from disruption (Fig. 5D–F).

In addition to the Western diet-like HFD model, inducing a metabolic disorder similar to mild human NASH, we also tested the MCDD model, which recapitulates more severe NASH pathologic features.[21] We first evaluated whether MCDD could induce perturbations in the GVB. Mice were fed an MCDD or chow diet for 1 week, and the expression of PV1 was evaluated in the ileum. As shown in Fig. S7, MCDD induced a marked upregulation of PV1 expression, which was corrected by OCA administration. These results indicate that MCDD also induces GVB damage and that OCA is also protective in this model.

To evaluate the therapeutic efficacy of OCA in ameliorating NASH, we administered the drug to mice fed with MCDD for 2 weeks, after the onset of liver damage assessed by increased ALT concentrations in the serum and lipid accumulation in the liver. OCA was then administered daily via oral gavage for the following 2 weeks in mice still fed MCDD (Fig. 6A). We observed that the upregulated PV1 expression induced by MCDD was restored by OCA in the ileum and colon, indicating its ability to seal a damaged GVB and to prevent further MCDD-induced damage (Fig. 6B,C). Moreover, 2 weeks of OCA treatment cured the liver damage, reducing ALT levels and lipid accumulation in the liver (Fig. 6D,E). These data suggest a role for OCA, likely via FXR activation, in controlling GVB integrity either indirectly via epithelial cells or directly through an effect on endothelial cells. Indeed, FXR is expressed in endothelial cells,[28] where it regulates inflammation,[28] vascular tension,[29] and improves erectile function.[30]

As GVB integrity is controlled by the WNT/β-catenin signaling pathway, we assessed whether OCA could activate this pathway. Primary endothelial cells were exposed to OCA and the expression of β-catenin downstream target genes was evaluated. As shown in Fig. S8, not only *Lef1* and *Ccdn1* β-catenin target genes were upregulated by OCA but also genes coding for tight junction proteins *Cldn5* and *Zo-1*. Collectively, these results indicate that OCA can directly target endothelial cells by activating the WNT/β-catenin signaling pathway and upregulating tight junction proteins, resulting in GVB protection and endothelial cell sealing.

Patients with NASH display GVB impairment

Having shown that GVB impairment is a prerequisite for NASH development, we analyzed whether we could also detect upregulation of PV1 in the intestines of patients with NASH. We tested PV1 expression on colonic biopsies obtained during colonoscopy of 9 patients with NASH (see demographic characteristics of NASH patients). As a control, we analyzed the healthy portion of colon from tumor bearing patients. As shown in Fig. 6F,G, patients with NASH displayed upregulation of PV1 in gut endothelial vessels, suggesting that the GVB is also compromised in the pathogenesis of NASH in humans.

Discussion

A role for the intestinal barrier in the development of liver disorders has been postulated, but several questions are still open.[14] It is not clear, for instance, if increased intestinal permeability is a cause or a consequence of liver disease, particularly in NASH.[9] Here, we have clearly connected the microbiota with increased epithelial and gut vascular permeability as well as with NASH development. We have shown that disruption of the GVB is an early event in NASH pathogenesis and is a consequence of diet-induced dysbiosis. Damage of the GVB is sustained as it is still observed in an inflammatory model of NASH (HFD 60%). We have also shown that GVB disruption is required for NASH development and that the GVB is a new target for pharmacologic intervention. We found that the FXR agonist OCA could activate the WNT/β-catenin signaling pathway and thus seal the GVB. Consistent with this observation, OCA administration during HFD feeding inhibited the upregulation of PV1 in the GVB and the subsequent increased permeability, and was also able to restore PV1 expression in the MCDD model. While MCDD is not a good model of obesity-induced NASH, as it is not associated with insulin resistance, a role of OCA in protection in an HFD-induced NASH model has recently been demonstrated in a therapeutic setting, indicating that FXR-engagement may be protective in several models where the GVB is disrupted.[31] OCA could act directly on endothelial cells or indirectly via epithelial cells to control PV1 expression and GVB function. However, the finding that mice deficient for FXR in the intestinal epithelium are not susceptible to NASH or liver steatosis,[32] suggests a role for endothelial FXR in controlling GVB permeability and NASH development. Consistent with this observation, and with a sustained disruption of the GVB, we also found that patients with NASH display a disrupted GVB, as demonstrated by increased PV1 expression on gut vessels.

Dysbiosis has been associated with several liver disorders, including NASH,[33,34] and a metagenomic signature with increased Proteobacteria and reduced Firmicutes is predictive of liver fibrosis in patients with NASH.[34] We show that microbiota from mice fed HFD for just 1 week was sufficient to disrupt the GVB and increase EAT when transplanted into standard diet-fed mice. Consistent with a role of the microbiota in NASH development, FMT from patients with NASH worsens diet-induced NASH in mouse models.[35] Similarly, the microbiota from mice with inflammasome deficiency exacerbate hepatic steatosis and inflammation through translocation of TLR4 and TLR9 agonists into the portal circulation in another model of NASH.[36] This is in line with our findings that HFD drives dysbiosis, leading to the impairment of the GVB, and subsequently the release of bacteria into the systemic circulation. As liver bacteria were not associated with CD45+ immune cells, we propose that they migrate freely into the liver after crossing first the IEB and entering the portal circulation through the damaged GVB.

We have shown that the capacity of bacteria to cross the GVB is an active mechanism which, in the case of *Salmonella typhimurium*, is dependent on the Salmonella pathogenicity island II.[13] Thus, it is likely that HFD-induced dysbiosis results in bacteria being able to cross a compromised GVB. We cannot exclude that there may be cooperation between microbes and that some may be capable of crossing the IEB, while others the GVB. Bacterial translocation during HFD may induce sustained inflammation, that together with the high content of lipids in the diet, may drive the metabolic disorder, leading to insulin resistance which is not observed in other NASH models. Alternatively, HFD has been shown to affect the composition of bile acids,[37] which may on one side change the microbiota composition,[38] and on the other affect the activation of FXR, with clear effects on barrier properties. It is likely that the modified microbiota may in turn change the bile acid composition, leading to an amplification of the effect.

In conclusion, these results indicate that increased intestinal permeability due to deranged GVB is responsible for the translocation of whole bacteria or bacterial products through the portal circulation into the liver, and eventually into the systemic circulation. By only protecting the GVB, through the activation of the WNT/β-catenin signaling pathway in endothelial cells, we can prevent NASH and the associated metabolic syndrome, pointing to the GVB as a new therapeutic target. However, as we could not control the activation of the WNT/β-catenin signaling pathway only in intestinal endothelial cells, we cannot exclude a concomitant effect of activation of this pathway in liver endothelium. This may contribute to control direct lipid access to the liver from the systemic circulation. This is unlikely as lipid absorption occurs mainly through chylomicrons, large lipoprotein particles unable to enter capillaries, but picked up by the lacteals, lymphatic capillaries that poke up into the center of each villus.[39]

We have shown that targeting the FXR with OCA can lead to activation of the WNT/β-catenin signaling pathway in endothelial cells and sealing of the GVB, even in a therapeutic setting, thus inhibiting further translocation of potentially harmful bacteria and their determinants, with clear effects on NASH control. This may contribute to explain the beneficial effects of OCA in patients with NASH.[20]

The beneficial effects of preserving IEB and GVB integrity may extend beyond liver disorders, as intestinal alterations and gut mucosal inflammation have also been observed in other systemic diseases.[40–44] A high percentage of patients with autism spectrum disorders,[40–44] for instance, and their first-degree relatives are characterized by increased intestinal permeability compared to healthy children.[45] Similarly, evidence suggests that increased gut permeability may precede or occur concomitantly with type I diabetes, as early evidence of the disease occurs in association with an enteropathy.[46,47] The higher permeability of the gut barrier may allow the uptake of dietary antigens, favoring autoimmunity.[48] Hence, understanding the role of the IEB and, in particular, of the GVB in other systemic disorders may lead to clinical benefit in the entire gut-liver-brain axis and may provide new opportunities for therapeutic intervention.

Financial support

This work was supported by Italian Association for Cancer Research AIRC (iCARE, JM), Swiss-National-Fund SNF (RW), European Research Council ERC (HomeoGUT No. 615735, MR), AIRC (MR) and Intercept Pharmaceuticals (MR).

Conflict of interest

Luciano Adorini works for Intercept Pharmaceuticals that provided obeticholic acid and part of financial support to this work.

Please refer to the accompanying ICMJE disclosure forms for further details.

Authors' contributions

JM, PB, IS, AS and MS designed, performed and analyzed experiments. EM performed experiments. JM, PB, IS and MR wrote the paper. RW, LA and GP helped in designing experiments and improving the manuscript. PI and MG provided human samples and scoring of the patients. JM and MR conceived and designed the study, analyzed and interpreted the data.

Acknowledgments

We thank Dr Paolo Magni and Dr Edina Hot for their help on experimental set up. We thank Dr Giulia Fornasa and Dr Milena Vitale for helping in experiments execution. We would like to thank Dr Luca Mazzarella for helpful discussions.

Supplementary data

Supplementary data to this article can be found online at https://doi.org/10.1016/j.jhep.2019.08.005.

References

Author names in bold designate shared co-first authorship

[1] Tanaka N, Aoyama T, Kimura S, Gonzalez FJ. Targeting nuclear receptors for the treatment of fatty liver disease. Pharmacol Ther 2017;179:142–157. https://doi.org/10.1016/j.pharmthera.2017.05.011.
[2] Cohen JC, Horton JD, Hobbs HH. Human fatty liver disease: old questions and new insights. Science 2011;332:1519–1523. https://doi.org/10.1126/science.1204265.
[3] Caligiuri A, Gentilini A, Marra F. Molecular pathogenesis of NASH. Int J Mol Sci 2016;17:1575. https://doi.org/10.3390/ijms17091575.
[4] Tilg H, Moschen AR. Evolution of inflammation in nonalcoholic fatty liver disease: the multiple parallel hits hypothesis. Hepatology 2010;52:1836–1846. https://doi.org/10.1002/hep.24001.

[5] Suzuki A, Diehl AM. Nonalcoholic steatohepatitis. Annu Rev Med 2017;68:85–98. https://doi.org/10.1146/annurev-med-051215-031109.
[6] Schnabl B, Brenner DA. Interactions between the intestinal microbiome and liver diseases. Gastroenterology 2014;146:1513–1524. https://doi.org/10.1053/j.gastro.2014.01.020.
[7] Boursier J, Diehl AM. Nonalcoholic fatty liver disease and the gut microbiome. Clin Liver Dis 2016;20:263–275. https://doi.org/10.1016/j.cld.2015.10.012.
[8] Fukui H. Gut-liver axis in liver cirrhosis: how to manage leaky gut and endotoxemia. World J Hepatol 2015;7:425–442. https://doi.org/10.4254/wjh.v7.i3.425.
[9] Miele L, Valenza V, La Torre G, Montalto M, Cammarota G, Ricci R, et al. Increased intestinal permeability and tight junction alterations in nonalcoholic fatty liver disease. Hepatology 2009;49:1877–1887. https://doi.org/10.1002/hep.22848.
[10] Buckley A, Turner JR. Cell biology of tight junction barrier regulation and mucosal disease. Cold Spring Harb Perspect Biol 2018;10. https://doi.org/10.1101/cshperspect.a029314 a029314.
[11] Rahman K, Desai C, Iyer SS, Thorn NE, Kumar P, Liu Y, et al. Loss of junctional adhesion molecule a promotes severe steatohepatitis in mice on a diet high in saturated fat, fructose, and cholesterol 733–746.e12. Gastroenterology 2016;151. https://doi.org/10.1053/j.gastro.2016.06.022.
[12] Johansson MEV, Sjövall H, Hansson GC. The gastrointestinal mucus system in health and disease. Nat Rev Gastroenterol Hepatol 2013;10:352–361. https://doi.org/10.1038/nrgastro.2013.35.
[13] Spadoni I, Zagato E, Bertocchi A, Paolinelli R, Hot E, Di Sabatino A, et al. A gut-vascular barrier controls the systemic dissemination of bacteria. Science 2015;350:830–834. https://doi.org/10.1126/science.aad0135.
[14] Spadoni I, Fornasa G, Rescigno M. Organ-specific protection mediated by cooperation between vascular and epithelial barriers. Nat Rev Immunol 2017;17:761–773. https://doi.org/10.1038/nri.2017.100.
[15] Ciccia F, Guggino G, Rizzo A, Alessandro R, Luchetti MM, Milling S, et al. Dysbiosis and zonulin upregulation alter gut epithelial and vascular barriers in patients with ankylosing spondylitis. Ann Rheum Dis 2017;76:1123–1132. https://doi.org/10.1136/annrheumdis-2016-210000.
[16] Pellicciari R, Fiorucci S, Camaioni E, Clerici C, Costantino G, Maloney PR, et al. 6α-Ethyl-chenodeoxycholic acid (6-ECDCA), a potent and selective FXR agonist endowed with anticholestatic activity. J Med Chem 2002;45:3569–3572. https://doi.org/10.1021/jm025529g.
[17] Gadaleta RM, van Erpecum KJ, Oldenburg B, Willemsen ECL, Renooij W, Murzilli S, et al. Farnesoid X receptor activation inhibits inflammation and preserves the intestinal barrier in inflammatory bowel disease. Gut 2011;60:463–472. https://doi.org/10.1136/gut.2010.212159.
[18] Verbeke L, Farre R, Verbinnen B, Covens K, Vanuytsel T, Verhaegen J, et al. The FXR agonist obeticholic acid prevents gut barrier dysfunction and bacterial translocation in cholestatic rats. Am J Pathol 2015;185:409–419. https://doi.org/10.1016/j.ajpath.2014.10.009.
[19] Mudaliar S, Henry RR, Sanyal AJ, Morrow L, Marschall H-U, Kipnes M, et al. Efficacy and safety of the farnesoid X receptor agonist obeticholic acid in patients with type 2 diabetes and nonalcoholic fatty liver disease 574-82.e1. Gastroenterology 2013;145. https://doi.org/10.1053/j.gastro.2013.05.042.
[20] Neuschwander-Tetri BA, Loomba R, Sanyal AJ, Lavine JE, Van Natta ML, Abdelmalek MF, et al. Farnesoid X nuclear receptor ligand obeticholic acid for non-cirrhotic, non-alcoholic steatohepatitis (FLINT): a multicentre, randomised, placebo-controlled trial. Lancet (London, England) 2015;385:956–965. https://doi.org/10.1016/S0140-6736(14)61933-4.
[21] Machado MV, Michelotti GA, Xie G, Almeida Pereira T, de Almeida TP, Boursier J, et al. Mouse models of diet-induced nonalcoholic steatohepatitis reproduce the heterogeneity of the human disease. PLoS One 2015;10. https://doi.org/10.1371/journal.pone.0127991 e0127991.
[22] Canto MI, Anandasabapathy S, Brugge W, Falk GW, Dunbar KB, Zhang Z, et al. In vivo endomicroscopy improves detection of Barrett's esophagus-related neoplasia: a multicenter international randomized controlled trial (with video). Gastrointest Endosc 2014;79:211–221. https://doi.org/10.1016/j.gie.2013.09.020.
[23] Macotela Y, Boucher J, Tran TT, Kahn CR. Sex and depot differences in adipocyte insulin sensitivity and glucose metabolism. Diabetes 2009;58:803–812. https://doi.org/10.2337/db08-1054.
[24] Neyrinck AM, Possemiers S, Verstraete W, De Backer F, Cani PD, Delzenne NM. Dietary modulation of clostridial cluster XIVa gut bacteria (Roseburia spp.) by chitin-glucan fiber improves host metabolic alterations induced by high-fat diet in mice. J Nutr Biochem 2012;23:51–59. https://doi.org/10.1016/j.jnutbio.2010.10.008.
[25] Rabot S, Membrez M, Bruneau A, Gérard P, Harach T, Moser M, et al. Germ-free C57BL/6J mice are resistant to high-fat-diet-induced insulin resistance and have altered cholesterol metabolism. FASEB J 2010;24:4948–4959. https://doi.org/10.1096/fj.10-164921.
[26] Jouihan H, Will S, Guionaud S, Boland ML, Oldham S, Ravn P, et al. Superior reductions in hepatic steatosis and fibrosis with co-administration of a glucagon-like peptide-1 receptor agonist and obeticholic acid in mice. Mol Metab 2017;6:1360–1370. https://doi.org/10.1016/j.molmet.2017.09.001.
[27] Úbeda M, Lario M, Muñoz L, Borrero M-J, Rodríguez-Serrano M, Sánchez-Díaz A-M, et al. Obeticholic acid reduces bacterial translocation and inhibits intestinal inflammation in cirrhotic rats. J Hepatol 2016;64:1049–1057. https://doi.org/10.1016/j.jhep.2015.12.010.
[28] Bishop-Bailey D, Walsh DT, Warner TD. Expression and activation of the farnesoid X receptor in the vasculature. Proc Natl Acad Sci 2004;101:3668–3673. https://doi.org/10.1073/pnas.0400046101.
[29] Zhang R, Ran H, Peng L, Zhang Y, Shen W, Sun T, et al. Farnesoid X receptor regulates vasoreactivity via Angiotensin II type 2 receptor and the kallikrein-kinin system in vascular endothelial cells. Clin Exp Pharmacol Physiol 2016;43:327–334. https://doi.org/10.1111/1440-1681.12535.
[30] Vignozzi L, Morelli A, Filippi S, Comeglio P, Chavalmane AK, Marchetta M, et al. Farnesoid X receptor activation improves erectile function in animal models of metabolic syndrome and diabetes. J Sex Med 2011;8:57–77. https://doi.org/10.1111/j.1743-6109.2010.02073.x.
[31] **Zhang D-Y**, **Zhu L**, **Liu H-N**, Tseng Y-J, Weng S-Q, Liu T-T, et al. The protective effect and mechanism of the FXR agonist obeticholic acid via targeting gut microbiota in non-alcoholic fatty liver disease. Drug Des Devel Ther 2019;13:2249–2270. https://doi.org/10.2147/DDDT.S207277.
[32] **Schmitt J**, **Kong B**, Stieger B, Tschopp O, Schultze SM, Rau M, et al. Protective effects of farnesoid X receptor (FXR) on hepatic lipid accumulation are mediated by hepatic FXR and independent of intestinal FGF15 signal. Liver Int 2015;35:1133–1144. https://doi.org/10.1111/liv.12456.
[33] Shen F, Zheng R-D, Sun X-Q, Ding W-J, Wang X-Y, Fan J-G. Gut microbiota dysbiosis in patients with non-alcoholic fatty liver disease. Hepatobiliary Pancreat Dis Int 2017;16:375–381. https://doi.org/10.1016/S1499-3872(17)60019-5.
[34] Loomba R, Seguritan V, Li W, Long T, Klitgord N, Bhatt A, et al. Gut Microbiome-based metagenomic signature for non-invasive detection of advanced fibrosis in human nonalcoholic fatty liver disease 1054–1062.e5. Cell Metab 2017;25. https://doi.org/10.1016/j.cmet.2017.04.001.
[35] Chiu C-C, Ching Y-H, Li Y-P, Liu J-Y, Huang Y-T, Huang Y-W, et al. Nonalcoholic fatty liver disease is exacerbated in high-fat diet-fed gnotobiotic mice by colonization with the gut microbiota from patients with nonalcoholic steatohepatitis. Nutrients 2017;9:1220. https://doi.org/10.3390/nu9111220.
[36] **Henao-Mejia J**, **Elinav E**, **Jin C**, Hao L, Mehal WZ, Strowig T, et al. Inflammasome-mediated dysbiosis regulates progression of NAFLD and obesity. Nature 2012;482:179–185. https://doi.org/10.1038/nature10809.
[37] La Frano MR, Hernandez-Carretero A, Weber N, Borkowski K, Pedersen TL, Osborn O, et al. Diet-induced obesity and weight loss alter bile acid concentrations and bile acid-sensitive gene expression in insulin target tissues of C57BL/6J mice. Nutr Res 2017;46:11–21. https://doi.org/10.1016/j.nutres.2017.07.006.
[38] Ramírez-Pérez O, Cruz-Ramón V, Chinchilla-López P, Méndez-Sánchez N. The role of the gut microbiota in bile acid metabolism. Ann Hepatol 2017;16:S21–S26. https://doi.org/10.5604/01.3001.0010.5672.
[39] Tso P, Pitts V, Granger DN. Role of lymph flow in intestinal chylomicron transport. Am J Physiol 1985;249:G21–G28. https://doi.org/10.1152/ajpgi.1985.249.1.G21.
[40] Fiorentino M, Sapone A, Senger S, Camhi SS, Kadzielski SM, Buie TM, et al. Blood-brain barrier and intestinal epithelial barrier alterations in autism spectrum disorders. Mol Autism 2016;7:49. https://doi.org/10.1186/s13229-016-0110-z.
[41] Horvath K, Perman JA. Autistic disorder and gastrointestinal disease. Curr Opin Pediatr 2002;14:583–587. https://doi.org/10.1097/00008480-200210000-00004.
[42] Ibrahim SH, Voigt RG, Katusic SK, Weaver AL, Barbaresi WJ. Incidence of gastrointestinal symptoms in children with autism: a population-based study. Pediatrics 2009;124:680–686. https://doi.org/10.1542/peds.2008-2933.

[43] Klukowski M, Wasilewska J, Lebensztejn D. Sleep and gastrointestinal disturbances in autism spectrum disorder in children. Dev Period Med n.d.;19:157–61.
[44] Kushak RI, Buie TM, Murray KF, Newburg DS, Chen C, Nestoridi E, et al. Evaluation of intestinal function in children with autism and gastrointestinal symptoms. J Pediatr Gastroenterol Nutr 2016;62:687–691. https://doi.org/10.1097/MPG.0000000000001174.
[45] de Magistris L, Familiari V, Pascotto A, Sapone A, Frolli A, Iardino P, et al. Alterations of the intestinal barrier in patients with autism spectrum disorders and in their first-degree relatives. J Pediatr Gastroenterol Nutr 2010;51:418–424. https://doi.org/10.1097/MPG.0b013e3181dcc4a5.
[46] Bosi E, Molteni L, Radaelli MG, Folini L, Fermo I, Bazzigaluppi E, et al. Increased intestinal permeability precedes clinical onset of type 1 diabetes. Diabetologia 2006;49:2824–2827. https://doi.org/10.1007/s00125-006-0465-3.
[47] Sapone A, de Magistris L, Pietzak M, Clemente MG, Tripathi A, Cucca F, et al. Zonulin upregulation is associated with increased gut permeability in subjects with type 1 diabetes and their relatives. Diabetes 2006;55:1443–1449. https://doi.org/10.2337/db05-1593.
[48] Ménard S, Cerf-Bensussan N, Heyman M. Multiple facets of intestinal permeability and epithelial handling of dietary antigens. Mucosal Immunol 2010;3:247–259. https://doi.org/10.1038/mi.2010.5.
[49] Harada N, Tamai Y, Ishikawa T, Sauer B, Takaku K, Oshima M, et al. Intestinal polyposis in mice with a dominant stable mutation of the beta-catenin gene. EMBO J 1999;18:5931–5942. https://doi.org/10.1093/emboj/18.21.5931.
[50] Kleiner DE, Brunt EM, Van Natta M, Behling C, Contos MJ, Cummings OW, et al. Design and validation of a histological scoring system for nonalcoholic fatty liver disease. Hepatology 2005;41:1313–1321. https://doi.org/10.1002/hep.20701.